Electronic Supplementary Material (ESI) for Reaction Chemistry & Engineering.

Supporting Information

Spatially resolved investigation into the coke formation and chemical states of nickel during autothermal reforming of acetic acid over Ni/CeO_2-ZrO_2 catalysts

Nat Phongprueksathat [a], Thanakorn Thanasujaree [b], Vissanu Meeyoo [a, c, *], Thirasak Rirksomboon [b]

[a)] Centre for Advanced Materials and Environmental Research, Mahanakorn University of Technology, Bangkok 10530, Thailand

[b)] The Petroleum and Petrochemical College, Chulalongkorn University, Bangkok 10330, Thailand

[c)] Nanotec–KMUTT Center of Excellence on Hybrid Nanomaterials for Alternative Energy, King Mongkut's University of Technology (KMUTT), Thonburi, Bangkok 10140, Thailand

Keywords: acetic acid; autothermal reforming; carbon formation; nickel; ceria; zirconia;

---

*To whom the correspondence should be addressed:

Mahanakorn University of Technology, Bangkok, Thailand 10530
Tel: +66(2)-988-4043; fax: +66(2)-2988-4039

Email address: vissanu@mut.ac.th (V.Meeyoo)

Contents

1. Experimental

1.1 Catalyst characterizations procedures

1.1.1 BET Surface Area

BET surface area is determined by N_2 adsorption at -196 °C using a Quantachrome Autosorb-1MP. Before the analysis, the samples are outgassed to eliminated volatile adsorbents on the surface at 250 °C for 12 h. The quantity of gas adsorbed onto or desorbed from a solid surface is measured at 5 equilibrium vapor pressure (P/P_o) values of 0.1115, 0.1615, 0.2115, 0.2615, and 0.3115 by the static volumetric method (Eq. 1). The adsorption data are calculated using Brunauer–Emmett–Teller (BET) method as shown in Eq. 2:

$$\frac{P/P_0}{W\left(1-P/P_0\right)} = \frac{1}{W_m C} + \frac{C-1}{W_m C}\left(P/P_0\right) \tag{1}$$

where

W = the weight of gas adsorbed at relative pressure P_0 (g)

W_m = the weight of adsorbate constituting a monolayer of surface coverage (g)

C = a constant that is related to the energy of adsorption in the first adsorbed layer and magnitude of adsorbate interaction and then the surface of the sample will be calculated by

$$\text{The surface area of the sample} = \frac{W_m A_{\text{nitrogen}} \left(6.02\times10^{23}\right)}{Mw_{\text{nitrogen}}} \tag{2}$$

where

$A_{nitrogen}$ = the crossed-section area of one molecule nitrogen = 0.162 nm^2 at -196 °C

$Mw_{nitrogen}$ = the molecular weight of nitrogen (g/mol)

1.1.2 H_2-Temperature Programmed Reduction

Temperature programmed reduction of hydrogen (H_2-TPR) is carried out using an SRI model 110 TCD detector. The samples are pretreated in an N_2 atmosphere at 150 °C for 30 min before running the TPR experiment and then cooled down to room temperature with N_2 feeding. A 5 % H_2/ N_2 gas is used as a reducing gas. The temperature is raised at a constant rate of 10 °C/min from room temperature to 900 °C. The amount of H_2 consumption as a function of temperature is determined from a TCD signal.

1.1.3 Temperature Programmed Oxidation (TPO)

The temperature Programmed Oxidation (TPO) technique is employed to analyze the amount and characteristics of the coke deposited on the spent catalyst. The spent catalyst is performed in a continuous flow of 5 % O_2 in He while the temperature will be linearly increased with a heating rate of 10 °C/min. The CO_2 produced by the oxidation of the coke species is converted to methane using a mechanized filled with 15%Ni/Al_2O_3 and operated at 415 °C in the presence of H_2. The evolution of methane is analyzed using an FID detector.

1.1.4 X-ray Diffraction (XRD)

A Rigagu X-ray diffractometer (XRD) system equipped with a RINT 2000 wide-angle goniometer using CuK_α radiation (1.5406 Å) and a power of 40 kV×30 mA is used for examination of the crystalline structure. The sample is ground to a fine homogeneous powder and held on a thin-walled glass plate against the X-ray beam. The intensity data is collected at 25 °C over a 2θ range of 20° to 80° with a scan speed of 5° (2θ)/min and a scan step of 0.02° (2θ).

1.1.5 X-Ray Fluorescence (XRF)

Ceria-Zirconia support is characterized by XRF-semi quantitative method over X-ray Fluorescence Analyzer (model: Panalytical Axios, PW 4400) to ensured that the support is completely synthesized and close to the desired Ce to Zr molar ratio of 3:1 and detected weight percent (wt%) of Ni metal at the catalyst surface.

1.1.6 X-ray Photoelectron Spectroscopy (XPS)

XPS is used for the determination of the surface composition, chemical state, and oxidation state of the fresh and spent catalysts. The XPS spectra are obtained by using an incident chromatic AlKα X-ray source (1253.6 eV) operated at 14.8 kV and 20 mA for excitation and a hemisphere analyzer (Thermo VG scientific). The high-resolution XPS spectra are the composite average of 10 scans with a passing energy of 50 eV. The pressure in the analysis chamber is in the range of 10^{-8} Torr during data collection. The binding energy is adjusted to the C 1s peak at 285 eV. Data analysis and curve de-convolution are accomplished by using the Thermo Advantage Spectra Data Processor software. The from the electron pass energy, the inelastic mean free path (IMFP) for Ni and C approximated from NIST Electron Inelastic-Mean-Free-Path Database are 4.8 and 5.8 Å, respectively. This can be translated to a sampling depth of 1.4-1.8 nm.

1.1.7 Scanning Electron Microscopy (SEM)

SEM imaging is carried out using a Tabletop microscope TM 3000 (Hitachi) operated at 5 kV and 15 mA and used for examination of the sample morphologies. Before scanning, the sample is dried overnight at 110 °C followed by Pt coating (model: E-1010) operated at 12 mA for 150 s.

1.1.8 Transmission Electron Microscopy (TEM)

The morphologies of carbon deposition are observed by transmission electron microscopy (TEM) with a JEOL (JEM-2100) transmission electron microscope operated at 200 kV. The samples are dispersed in absolute ethanol ultrasonically, and the solutions are dropped on copper grids coated with a lacey carbon film.

1.1.9 Thermogravimetric and Differential Thermal Analysis (TG-DTA)

Perkin-Elmer/Pyris Diamond TG-DTA instrument is used to study the thermal decomposition of coke to investigate a type of carbon species deposition. Each spent catalyst is heated to 800 °C with a ramping rate of 10 °C/min in the O_2 atmosphere (20 mL/min flow rate).

2. Results and discussion

2.1 Characterization of fresh catalyst

The BET surface areas and the XRD mean crystallite size of the catalysts are shown in Table S1 (Supporting information). The Ce/Zr molar ratio of the prepared $Ce_{0.75}Z_{0.25}O_2$ support has met the desired ratio of 3:1 and loading nickel metal are expected ca. 15 wt%. The surface area of Ni/ $Ce_{0.75}Z_{0.25}O_2$ catalyst and $Ce_{0.75}Z_{0.25}O_2$ support are ca. 75 and 96 m^2/g, respectively. The surface areas of Ni/ $Ce_{0.75}Z_{0.25}O_2$ catalyst are decreased as compared with that of $Ce_{0.75}Z_{0.25}O_2$ support due to a blockage of micropores by NiO particles. [1]

Table S1 The chemical compositions and BET surface areas of the support and catalyst synthesized

Catalyst	Composition[a] (wt%)				Ce/Zr ratio	BET surface area (m^2/g)	Mean Crystallite Size of Ni[b] (nm)
	Ce	Zr	Ni	O			
$Ce_{0.75}Zr_{0.25}O_2$	68.94	14.53	-	16.52	3.09:1	96	n/a
15wt% Ni/$Ce_{0.75}Zr_{0.25}O_2$	60.87	13.21	15.14	10.77	3.00:1	74	24.2 (111)[c]

[a] XRF technique

[b] Calculated from Scherrer equation
[c] Miller indices

The XRD patterns of Ni/$Ce_{0.75}Z_{0.25}O_2$ and $Ce_{0.75}Z_{0.25}O_2$ support are shown in Fig. 2, showing a typical dominant cubic fluorite structure of CeO_2 assigned to peaks of 28.6, 33.1, 47.4, and 56.4° indicating that a typical solid solution of $Ce_{0.75}Z_{0.25}O_2$ is formed. Besides, some extra peaks of the tetragonal phase of ZrO_2 were observed at 30.11, 50.23, and 59.48° indicating some of ZrO_2 were not incorporated in the CeO_2 lattice to form a solid solution. The presence of NiO is found on Ni/$Ce_{0.75}Zr_{0.25}O_2$ catalyst revealing peaks at 37.3, 43.3, 63.0, and 75.5° corresponding to plane indices of (111), (200), (220), and (311), respectively. The crystallite size of the Ni particle in the plane (111) is estimated to be ca. 24.2 nm using Scherrer equation.

The morphologies of $Ce_{0.75}Z_{0.25}O_2$ support and Ni/$Ce_{0.75}Z_{0.25}O_2$ catalyst are observed by Scanning Electron Microscopy (SEM) are presented in Fig. S2. All of which illustrates the aggregation of the primary long thin needle-shaped particles similar to that described by Thammachart *et al*.[2] In the presence of Ni metal, the fine particles of NiO can be observed as the attached on the surface of the long thin needles of the $Ce_{0.75}Z_{0.25}O_2$ support.

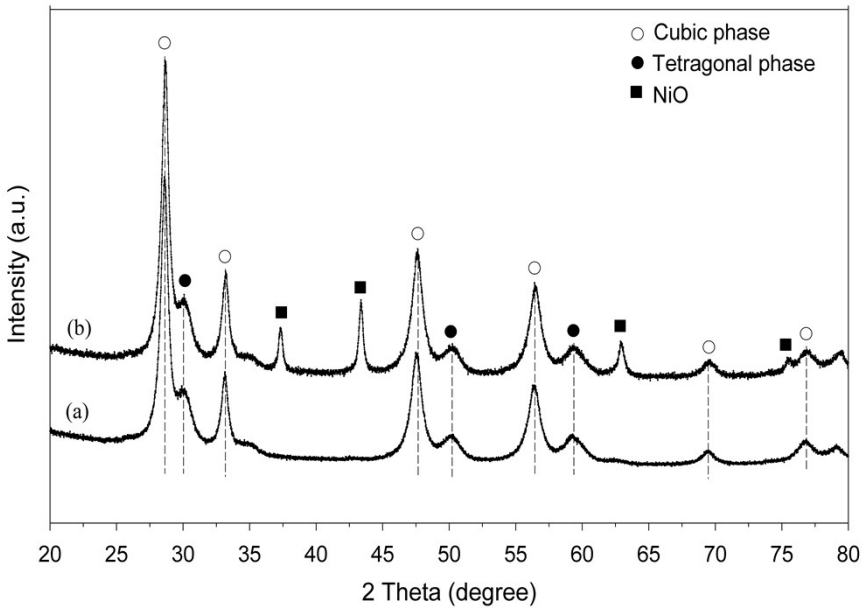

Figure S1. XRD patterns of catalysts calcined at 500 °C: (a) $Ce_{0.75}Zr_{0.25}O_2$ and (b) 15wt% Ni/$Ce_{0.75}Zr_{0.25}O_2$.

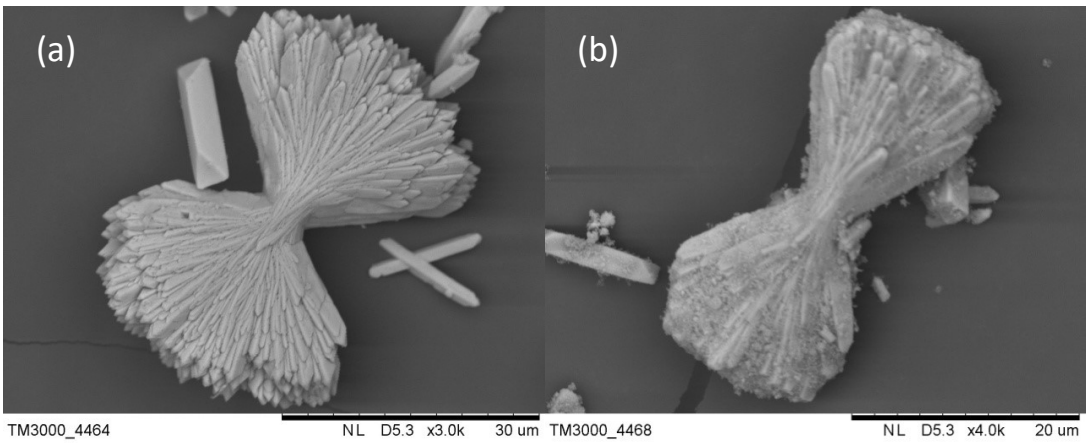

Figure S2 SEM images of (a) $Ce_{0.75}Zr_{0.25}O_2$ and (b) 15wt% Ni/$Ce_{0.75}Zr_{0.25}O_2$.

The H_2-TPR profiles of Ni/$Ce_{0.75}Zr_{0.25}O_2$ catalyst and $Ce_{0.75}Zr_{0.25}O_2$ support are shown in Fig. 3. The $Ce_{0.75}Zr_{0.25}O_2$ support exhibits two reduction peaks at 410 and 800 °C, which attribute to surface reduction and bulk reduction of CeO_2 from Ce^{4+} to Ce^{3+}, respectively. The Ni/$Ce_{0.75}Zr_{0.25}O_2$ catalyst exhibits two additional peaks from the $Ce_{0.75}Zr_{0.25}O_2$ support at 270 and 370 °C, which attribute to the reduction of free NiO particle and reduction of NiO interacting with $Ce_{0.75}Zr_{0.25}O_2$ support, respectively [3]. Similar reduction behavior of NiO is observed in the previous work.[4]

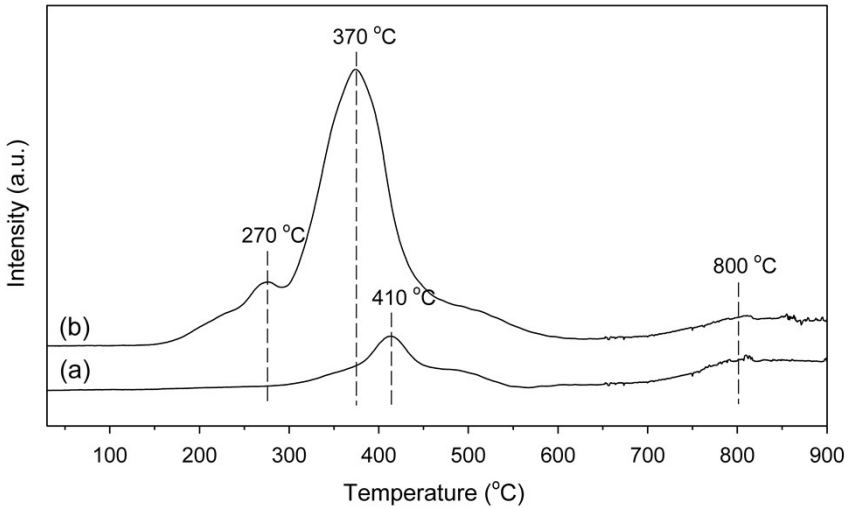

Figure S3. H_2-TPR profiles of catalysts with a heating rate of 10 °C/min, a reducing gas containing 5% H_2 in N_2 with a flow rate of 20 ml/min: (a) $Ce_{0.75}Zr_{0.25}O_2$ and (b) Ni/$Ce_{0.75}Zr_{0.25}O_2$.

2.2 *Catalytic activity*

Table S2 Catalytic activity for SR, POX, and ATR over $Ce_{0.75}Zr_{0.25}O_2$ and quartz wool at 650 °C, W/F = 0.352 g·hr/mol (Zone 4).

Parameters	$Ce_{0.75}Zr_{0.25}O_2$			Quartz Wool		
	SR	POX	ATR	SR	POX	ATR
CH_3COOH conversion (%)	65.2	11.3	67.0	1.43	1.62	1.3
O_2 conversion (%)	-	26.6	40.3	-	4.1	5.8
H_2 Yield (%)	32.7	2.2	19.5	0.6	0.1	0.3
CO Yield (%)	4.1	0.2	3.2	0.2	0.1	0.1
CO_2 Yield (%)	39.3	2.9	34.3	0.7	0.4	0.7
CH_4 Yield (%)	0.6	1.3	0.5	0.2	0.2	0.1
CH_3COCH_3 Yield (%)	3.0	3.1	2.9	0.7	0.6	0.6

Table S3 Catalytic activity for SR, POX, and ATR over $Ni/Ce_{0.75}Zr_{0.25}O_2$ at 650 °C and W/F of 0.088-0.352 g·hr/mol (Zone 1-4).

Conditions	SR				POX				ATR			
Zone	1	2	3	4	1	2	3	4	1	2	3	4
W/F (g·hr/mol)	0.088	0.176	0.264	0.352	0.088	0.176	0.264	0.352	0.088	0.176	0.264	0.352
CH_3COOH conversion (%)	78.6	95.9	100.0	100.0	19.8	24.6	29.2	30.4	66.6	93.0	100.0	100.0
O_2 conversion (%)	-	-	-	-	95.0	99.6	100.0	100.0	90.0	98.3	100.0	100.0
H_2 Yield (%)	63.3	78.7	89.2	89.5	14.1	18.0	23.6	26.6	49.2	68.4	79.0	79.4
CO Yield (%)	6.2	10.2	12.6	11.9	1.8	2.9	3.8	4.0	4.5	9.8	11.2	10.9
CO_2 Yield (%)	35.8	55.0	68.0	68.5	6.1	6.6	7.6	7.9	45.6	50.2	74.0	74.8
CH_4 Yield (%)	0.5	0.0	0.0	0.0	0.3	0.8	1.4	1.3	1.0	0.5	0.0	0.0
CH_3COCH_3 Yield (%)	4.2	1.0	0.0	0.0	2.0	1.3	0.1	0.0	3.7	0.9	0.0	0.0
C–C bond cleavage (%)[a]	42.5	65.2	80.6	80.4	8.2	10.3	12.8	13.2	51.1	60.5	85.2	85.7

[a] C–C bond cleavage conversion, $X_{C-C\ bond}$ (%) = $\frac{F_{CH_4,\,out} + F_{CO,\,out} + F_{CO_2,\,out}}{2 \times F_{AcOH,\,in}} \times 100$

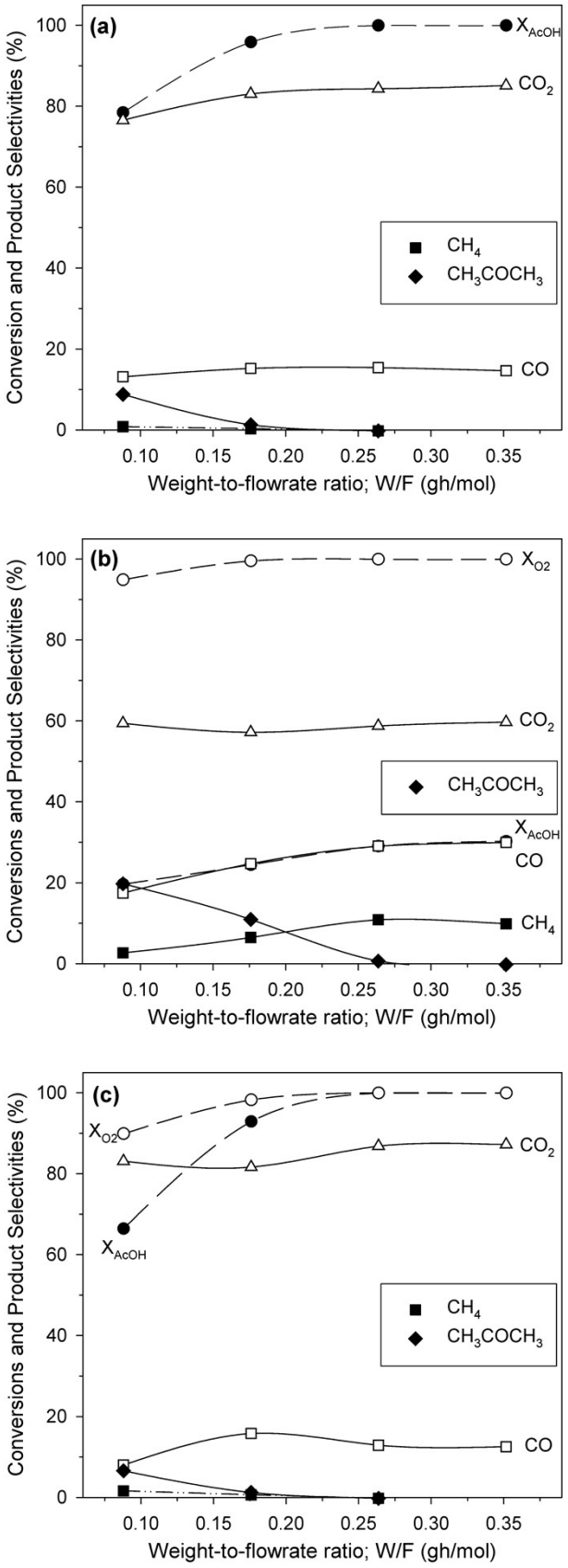

Figure S4. Conversions and selectivites from acetic acid reformings as a function of weight-to-flowrate ratio (W/F) over $Ni/Ce_{0.75}Zr_{0.25}O_2$ under (a) SR, (b) POX and (c) ATR conditions (T = 650 °C, S/C = 6, O/C = 0.175, F_{total} = 170 ml/min and TOS = 3 hr).

2.3 *Characterization of spent catalysts*

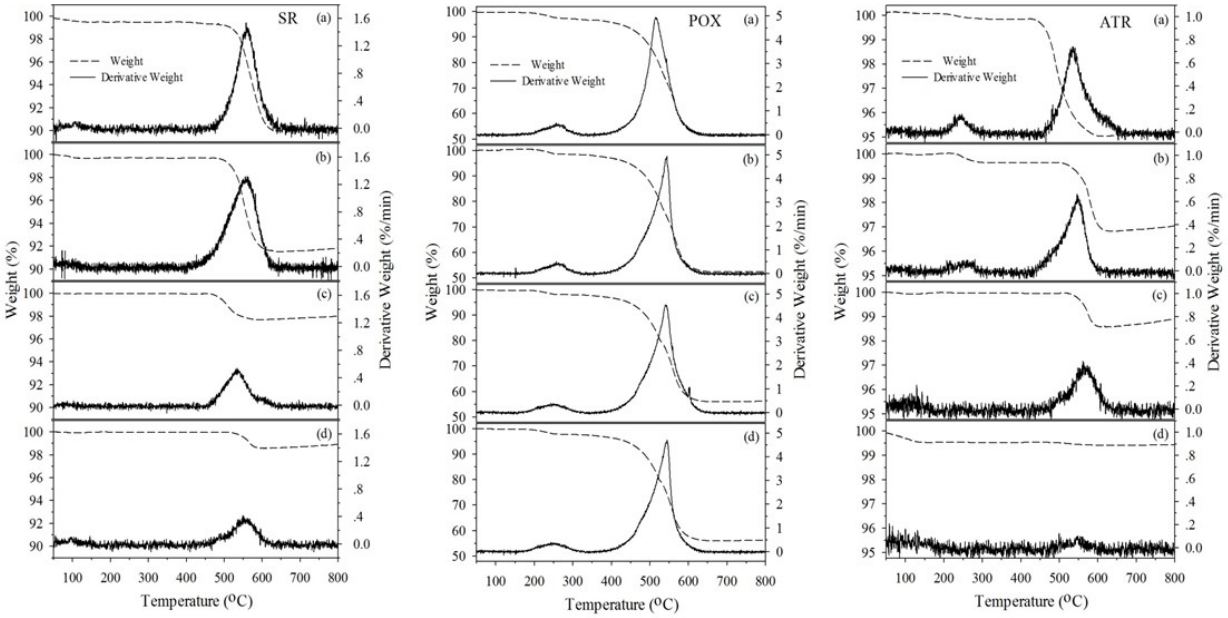

Figure S5. TG-DTA profiles of the spent Ni/$Ce_{0.75}Zr_{0.25}O_2$ catalyst under different processes (SR, POX, and ATR) with a heating rate of 10 °C/min, an oxidizing gas containing O2 in N2 with a flow rate of 20 ml/min at W/F of (a) 0.088, (b) 0.176, (c) 0.264, and (d) 0.352 g·hr/mol.

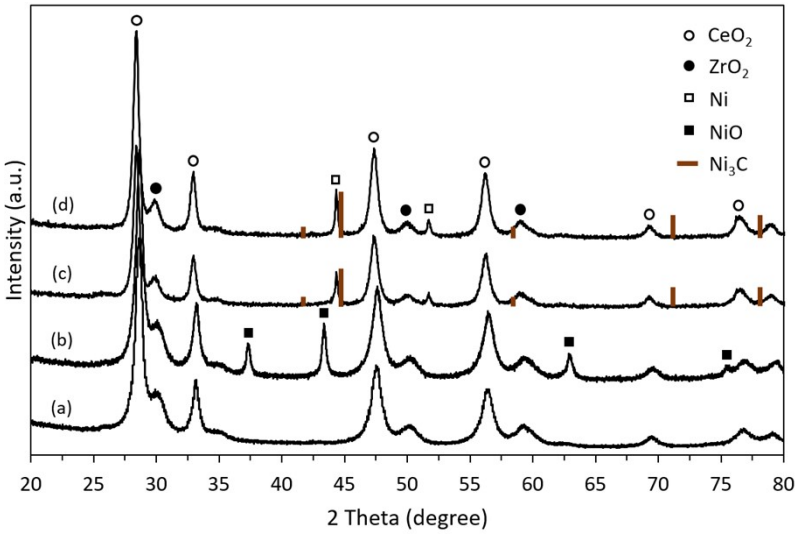

Figure S6. XRD patterns of the (a) fresh $Ce_{0.75}Zr_{0.25}O_2$, (b) fresh Ni/$Ce_{0.75}Zr_{0.25}O_2$, (c) spent Ni/$Ce_{0.75}Zr_{0.25}O_2$ in zone 1 from ATR, and (d) spent Ni/$Ce_{0.75}Zr_{0.25}O_2$ in zone 4 from ATR. Ni_3C was not detected as shown in the designated positions.

References

1 P. G. M. Assaf, F. G. E. Nogueira and E. M. Assaf, *Catalysis Today*, 2013, **213**, 2–8.

2 M. Thammachart, V. Meeyoo, T. Risksomboon and S. Osuwan, *Catalysis Today*, 2001, **68**, 53–61.

3 S. Pengpanich, V. Meeyoo and T. Rirksomboon, *Catalysis Today*, 2004, **93–95**, 95–105.

4 N. Phongprueksathat, V. Meeyoo and T. Rirksomboon, *International Journal of Hydrogen Energy*, 2019, **44**, 9359–9367.